

THE COSMIC GRAPH: OPTIMAL INFORMATION EXTRACTION FROM LARGE-SCALE STRUCTURE USING CATALOGUES

T. LUCAS MAKINEN

Imperial Centre for Inference and Cosmology (ICIC) & Astrophysics Group, Imperial College London, Blackett Laboratory, Prince Consort Road, London SW7 2AZ, United Kingdom and
Harvard & Smithsonian Center for Astrophysics, Observatory Building E, 60 Garden St, Cambridge, MA 02138, United States

TOM CHARNOCK

Freelance consultant in statistical modelling

PABLO LEMOS

Department of Physics and Astronomy, University of Sussex, Brighton, BN1 9QH, UK and
University College London, Gower St, London, UK

NATALIA PORQUERES & ALAN HEAVENS

Imperial Centre for Inference and Cosmology (ICIC) & Astrophysics Group, Imperial College London, Blackett Laboratory, Prince Consort Road, London SW7 2AZ, United Kingdom

BENJAMIN D. WANDELT

Sorbonne Université, CNRS, UMR 7095, Institut d’Astrophysique de Paris, 98 bis boulevard Arago, 75014 Paris, France and
Center for Computational Astrophysics, Flatiron Institute, 162 5th Avenue, New York, NY 10010, USA

Version December 23, 2022

ABSTRACT

We present an implicit likelihood approach to quantifying cosmological information over discrete catalogue data, assembled as graphs. To do so, we explore cosmological parameter constraints using mock dark matter halo catalogues. We employ Information Maximising Neural Networks (IMNNs) to quantify Fisher information extraction as a function of graph representation. We a) demonstrate the high sensitivity of modular graph structure to the underlying cosmology in the noise-free limit, b) show that graph neural network summaries automatically combine mass and clustering information through comparisons to traditional statistics, c) demonstrate that networks can still extract information when catalogues are subject to noisy survey cuts, and d) illustrate how nonlinear IMNN summaries can be used as asymptotically optimal compressed statistics for Bayesian simulation-based inference. We reduce the area of joint Ω_m, σ_8 parameter constraints with small (~ 100 object) halo catalogues by a factor of 42 over the two-point correlation function, and demonstrate that the networks automatically combine mass and clustering information. This work utilizes a new IMNN implementation over graph data in Jax, which can take advantage of either numerical or auto-differentiability. We also show that graph IMNNs successfully compress simulations away from the fiducial model at which the network is fitted, indicating a promising alternative to n -point statistics in catalogue simulation-based analyses.

Subject headings: cosmology, large-scale structure, statistical methods, machine learning, graph networks, galaxy surveys

1. INTRODUCTION

Modern cosmological analyses typically focus on obtaining theory and parameter constraints from compressed summary statistics obtained from field data such as the Cosmic Microwave Background or weak lensing mass-maps (Tegmark et al. 1997; Alsing & Wandelt 2018; Jeffrey et al. 2020). Recently, field-level analyses like Porqueres et al. (2021); Leclercq & Heavens (2021), although computationally expensive, have made it possible to sample the full field at the pixel level to ensure all survey information is accounted for in posterior construction for cosmological parameters.

However, the data collected by telescopes are often in-

stantly compressed into discrete catalogues of sources, like galaxies and their underlying dark matter halos, or cosmic voids (Sutter et al. 2012; Kreisch et al. 2021). The typical approach taken to analyse galaxy cluster data is to “paint” identified sources onto a grid and perform luminosity peak counts in high-density regions as a tracer for underlying dark matter. Analyses of these catalogues usually focus on 2-point information, either in real or Fourier space. However, these statistics are only sufficient when the underlying field is Gaussian, which is not the case for late-time cosmic web structures. Finding a statistic with which to capture more of this information is an active area of research. Existing methods include the three-point correlation function (the bispectrum in Fourier space, e.g. Philcox & Ivanov (2022)), Minkowski functionals (Petri et al. 2013), the

1D probability distribution function (Uhlemann et al. 2020), marked power spectra (Massara et al. 2022), minimum spanning trees (Barrow et al. 1985; Naidoo et al. 2019, 2022), and field-level sampling (Jasche & Wandelt 2013; Ramanah et al. 2019; Porqueres et al. 2021; Leclercq & Heavens 2021; Leclercq 2015; Jasche et al. 2015). However, truncating analyses to power or bispectra almost certainly discards information, especially for highly non-Gaussian fields, while field-level methods quickly become computationally expensive with increasing survey volume. Likewise, void cosmology constructs correlation functions from void positions and redshifts (Hamaus et al. 2015) to capture under-dense regions in structure formation. This sort of analysis usually discards morphological features of voids, such as void ellipticity, resulting in a loss of information that could be relevant to the underlying cosmological model (Biswas et al. 2010; Lavaux & Wandelt 2010; Xu et al. 2019).

Graphs provide a natural way to describe the nonlinear aspects of large-scale structure (LSS). Dark matter halos and their galaxy clusters can be attributed to nodes (vertices), while filaments are traced by smaller halos and edges connecting neighbouring edges. In this representation, clustering under gravity can be translated into higher connectivity or number of edges. Higher order n -point functions can be computed efficiently for clusters, while avoiding the cost of computing extraneous connections across voids. Graph representation of LSS promises a more modular approach to information quantification, and compliments the existing body of literature. Minimum spanning trees (MSTs) have been used in cosmological analyses since Barrow et al. (1985), and subsequent studies have investigated using binned halo graph features from simulations as cosmological probes (Bhavasar & Ling 1988; van de Weygaert et al. 1992; Krzewina & Saslaw 1996; Ueda & Itoh 1997; Coles et al. 1998; Adami & Mazure 1999; Colberg 2007; Alpaslan et al. 2014; Beuret et al. 2017; Libeskind et al. 2018; Bonnaire et al. 2020, 2022). More recently, Naidoo et al. (2022, 2019) use the minimum spanning tree (MST) computed from the *Quijote* simulations to compute the cosmological information by binning branch and shape features of the MST computed over the simulation suite. Yang & Yu (2022) illustrate graph-based approaches for modelling small-scale halo clustering in cosmological simulations.

The advent of deep learning in cosmology has made massive data generation and analysis more tractable. Many studies have investigated neural techniques for point estimate cosmological parameter extraction from cosmological fields via regression networks trained on simulation-parameter pairs (Pan et al. 2020; Ravanbakhsh et al. 2017; Kwon et al. 2020; Prelogović et al. 2021; Fluri et al. 2019, 2018; Matilla et al. 2020; Ribli et al. 2018; Gillet et al. 2019), field reconstruction (Dai & Seljak 2022; Jamieson et al. 2022), foreground removal emulation (Makinen et al. 2020; Jeffrey et al. 2022), or cosmological parameters from graphs (Villanueva-Domingo & Villaescusa-Navarro 2022) with squared loss. As reviewed in Villaescusa-Navarro et al. (2020a), these techniques can estimate the posterior mean of parameters (see also Jeffrey & Wandelt (2020)). This implies they require simulations drawn from a prior, specified at the time of training, not just near the parameters favored by the data. This adds to the variability that needs to

be fit by the network.

We take a different approach: we consider halo catalogue graphs as our dataset and use Information Maximising Neural Networks (IMNNs) to measure the Fisher information contained in these graphs. IMNNs are neural networks that compress data to informative nonlinear summaries, trained on simulations around a fiducial model to maximise the Fisher information (Charnock et al. 2018; Makinen et al. 2021), where, for the purposes of compression and forecasting only, the summary statistics are assumed to have a Gaussian sampling distribution. Neural networks can make use of all available data simultaneously, even saturating known field-level likelihoods (Makinen et al. 2021). This approach enables us to use asymptotically optimal nonlinear statistics (Alsing & Wandelt 2018; Charnock et al. 2018) to then compute summaries and estimate maximum likelihood parameters and perform efficient implicit likelihood inference over a prior.

We combine this framework with a graph neural network (GNN) architecture. GNNs are well-suited to discrete and variable-length problems such as molecular classification, weather forecasting, and even physics (re-)discovery with symbolic regression (Lemos et al. 2022; Cranmer et al. 2020), (see Battaglia et al. (2018) for a complete review).

Recent studies have made use of IMNNs for cosmology (Makinen et al. 2021; Fluri et al. 2021; Fluri et al. 2022), and highly non-Gaussian problems, such as galaxy type identification from multiband images (Livet et al. 2021). However, previous implementations relied on computing Fisher statistics for data with a *fixed input size*. Here, using GNNs, we extend the framework to a much more general class of problems. We will refer to graph IMNNs as gIMNNs.

We show how gIMNN summaries from catalogue graphs compares to traditional cosmological techniques *with respect to information extraction* using the *Quijote* halo catalogues (Villaescusa-Navarro et al. 2020b). We illustrate that by encoding physical symmetries and more descriptive graph attributes in the IMNN framework, we can extract more information from limited catalogues than traditional 2-point statistics.

The study is organised as follows: We present a graph description of large-scale structure in Section 2, followed by a review of the IMNN framework in the context of graph data in Section 3. In Section 4 we present our halo catalogue graph and GNN architectures and our main findings: We first investigate information as a function of increasing GNN depth and graph connectivity on both invariant and non-invariant graphs, and show that gIMNNs consistently extract more information than the 2-pt function. We next show that decorating graph nodes with mass further increases information extraction. Third, we explore the information stored in graph cardinality (the number of nodes or objects and edges connecting them) in the context of the halo mass function. Next, we proceed to a more realistic case in which catalogue construction is subject to various levels of uncertainty in the halo mass determination. In Section 7 we conclude by showing how trained gIMNN summaries can be used as optimal compressors in simulation-based inference density estimation. We include supplementary descriptions of graph assembly and network generaliza-

tion in Appendix B.

2. LARGE-SCALE STRUCTURE AS A GRAPH

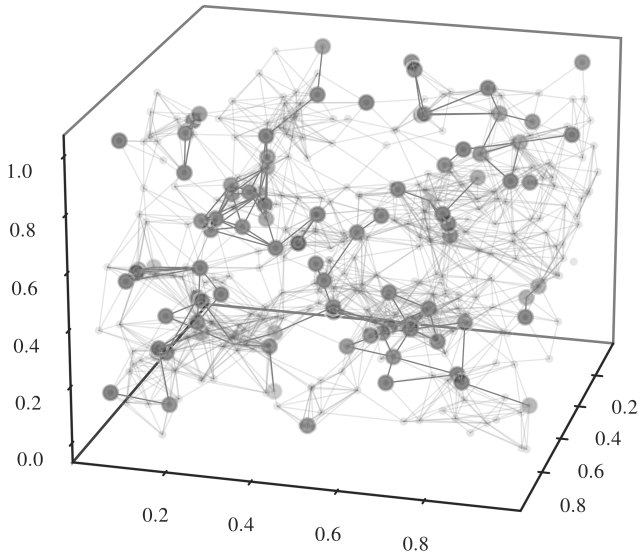


FIG. 1.— Dark matter halo graph representation of large-scale structure, constructed from a single *Quijote* simulation. The largest halos (grey) with a mass $M_i > 1.5 \times 10^{15} M_\odot$ trace the largest physical scales, here shown coloured by the log of the halo’s mass, and connected to all neighbours within a radius of $r_{\text{connect}} = 200$ Mpc. Smaller halo masses $M_i > 1.1 \times 10^{15} M_\odot$ (light grey) trace smaller scale clustering. The box encases a cosmological comoving volume of $(1\text{Gpc})^3$.

Graphs provide a natural language with which to describe the cosmic web. Dark matter halos are attributed to nodes (vertices), while filaments are traced by smaller halos and edges, illustrated in Figure 1. In this representation, clustering under gravitational interactions can be translated into higher edge cardinality (number of edges). Higher order n -point functions can be computed efficiently for clusters, while avoiding the cost of computing extraneous connections across voids. Void catalogues (where edges would correspond to the walls separating the voids) can likewise be assembled into the dual of a halo graph. Graph construction also allows arbitrary extra information, such as the halo masses or peculiar velocities, for which the underlying sampling distribution is not known, to be combined in a nonlinear fashion in the form of node or edge labels, unlike (marked) correlation functions.

2.1. Graph Notation

We define a graph explicitly as a tuple $G = (\mathbf{u}, V, E)$, following the notation in Battaglia et al. (2018). The \mathbf{u} is a global attribute of the graph, i.e. a label or global parameter value. $V = \{\mathbf{v}_i\}_{i=1:N^v}$ is the set of graph nodes, with cardinality N^v . The edge set $E = \{(\mathbf{e}_k, r_k, s_k)\}_{r_k=i, k=1:N^e}$, indexed by $k = 1 : N^e$, is comprised of vectors \mathbf{e}_k of cardinality N^e , which may be directed, connected via receiving and sending indices between nodes, r_k and s_k . Senders and receivers can be equivalently parameterized by an adjacency matrix A_{ij} in which i and j index sender and receiver nodes, respectively. Each node, indexed by $i = 1 : N^v$, has a set of

edges, $E'_i = \{(\mathbf{e}'_k, r_k, s_k)\}_{r_k=i, k=1:N^e}$, connected to it via a subset of senders and receivers. The full set of nodes is defined as $V = \{\mathbf{v}_i\}_{i=1:N^v}$, where each node \mathbf{v}_i is a vector of features. In a physical system of particles, one might represent V as a set of individual particles’ attributes, like mass, position, and velocity, with edges expressing interactions, such as forces, between particles. A global attribute of a graph might be a classification label, such as in molecule or cluster classification (Satorras et al. 2021; Kipf & Welling 2016). Careful data representation on graphs can vastly simplify physical problems via inductive biases and symmetry capture (see e.g. Lemos et al. 2022; Cranmer et al. 2020; Battaglia et al. 2018).

2.2. Halo Graphs

We define a dark matter halo graph $G = (\mathbf{u}, V^{\text{halo}}, E^{\text{halo}})$, constructed from a catalogue for a single realisation of the universe. We can equivalently define its dual, $H = (\mathbf{u}, V^{\text{void}}, E^{\text{void}})$, from a void catalogue. Note that if we assign global cosmological parameters to \mathbf{u} , G and H share this property. Hereafter we will focus on graphs from halo catalogues.

The graph framework allows the cardinality of a cosmological graph’s nodes and edges to vary as a function of cosmological or survey parameters, reflecting the often strong dependence of the abundance of clusters on cosmological parameters. When assembling a graph from a halo catalogue, we choose to vary two physical parameters: a mass cut, M_{cut} , and a linking radius, r_{connect} . A halo i with a mass above M_{cut} is connected to a halo j if the absolute distance between halos i and j is less than r_{connect} , i.e. $|\mathbf{d}_{ij}| < r_{\text{connect}}$. We display the same catalogue at two mass cuts in Figure 1. A conservative $M_{\text{cut}} = 1.5 \times 10^{15} M_\odot$ (dark points) contains the heaviest halos and traces the largest scales, while smaller masses ($M_{\text{cut}} = 1.1 \times 10^{15} M_\odot$, light points) trace smaller scales. Each graph is connected by $r_{\text{connect}} = 200$ Mpc.

Graphs can be assembled from halo catalogues in one of two ways: as non-invariant or as invariant graphs. Non-invariant graphs have positions, \mathbf{p} , as node labels, setting $\mathbf{v}_i = \mathbf{p}_i$, with edges labelled as the relative distances between halos, \mathbf{d}_{ij} . This graph is *not* invariant under translations and rotations, as the node values are pinned to the underlying simulation grid. *Invariant* graphs have only *relative* positional information, all of which is stored in the edges. The cosmological models that we wish to constrain are invariant to rigid Euclidean group rotations and translations of the large-scale structure. In this work we include both representations for completeness.

2.2.1. Node features

In the invariant representation, graph nodes are ‘decorated’ with either an indicator $\mathbf{v}_i = v_i = 1$ in the undecorated case or the halo’s scalar mass, $\mathbf{v}_i = v_i = M_i$. In the non-invariant case, nodes are also decorated with position $\mathbf{v}_i = (M_i, \mathbf{p}_i)$. We describe graph construction and padding details in Appendix B.

2.2.2. Edge features

To construct invariant graphs, we impose translational symmetry by attributing functions of relative positions between halos on the edges. We compute the vector separations $\mathbf{d}_{ij} = \mathbf{p}_i - \mathbf{p}_j$ between all halos and do not

link halos directly if $|\mathbf{d}_{ij}| > r_{\text{connect}}$. For rotational invariance, we adopt Villanueva-Domingo & Villaescusa-Navarro (2022)’s notation and first compute the unit vectors $\mathbf{s}_{ij} = \mathbf{d}_{ij}/|\mathbf{d}_{ij}|$ and $\mathbf{n}_i = (\mathbf{p}_i - \bar{\mathbf{p}})/|\mathbf{p}_i - \bar{\mathbf{p}}|$ where $\bar{\mathbf{p}}$ is the centroid (or reference halo position). We then compute the direction cosines $a_{ij} = \mathbf{n}_i \cdot \mathbf{n}_j$ and $b_{ij} = \mathbf{n}_i \cdot \mathbf{s}_{ij}$. The normalized edge features for *invariant* halo graphs are then

$$\mathbf{e}_{ij} = [|\mathbf{d}_{ij}|/r_{\text{connect}}, a_{ij}, b_{ij}], \quad (1)$$

whilst for non-invariant graphs, $\mathbf{e}_{ij} = |\mathbf{d}_{ij}|/r_{\text{connect}}$.

2.2.3. Global features

A halo graph’s global features can be any quantity that describes the global properties of the system, in this case configuration or cosmology parameters. In a regression case, one might wish to label each halo graph simulation with a set of cosmological or hydrodynamical parameters, as done in Villanueva-Domingo & Villaescusa-Navarro (2022), and fit a neural network to minimise some distance measure between the network output and these parameters. Here, global properties will be *arbitrary nonlinear summaries* of cosmology, learned in an unsupervised manner as a function of the graph’s attributes using information maximising neural networks.

3. INFORMATION MAXIMISING NEURAL NETWORKS

The graph framework allows for a modular study of the cosmological information embedded in large-scale structure. We next review IMNNs as a tool for information extraction, as well as optimal compression for graphs assembled from cosmological surveys. The IMNN framework is presented in full in Charnock et al. (2018) with developmental updates discussed in Makinen et al. (2021), but we review the formalism here for completeness and introduce new aspects to the technique. The sharper the peak of an informative likelihood function $\mathcal{L}(\mathbf{d}|\boldsymbol{\theta})$ for some fixed data \mathbf{d} with $n_{\mathbf{d}}$ data points and $n_{\boldsymbol{\theta}}$ parameters at a given value of $\boldsymbol{\theta}$, the more informative $\boldsymbol{\theta}$ is about the data. The Fisher information matrix describes how much information \mathbf{d} contains about the parameters, and is given as the second moment of the score of the likelihood

$$\mathbf{F}_{\alpha\beta} = \int d\mathbf{d} \mathcal{L}(\mathbf{d}|\boldsymbol{\theta}) \frac{\partial \ln \mathcal{L}(\mathbf{d}|\boldsymbol{\theta})}{\partial \theta_{\alpha}} \frac{\partial \ln \mathcal{L}(\mathbf{d}|\boldsymbol{\theta})}{\partial \theta_{\beta}}, \quad (2)$$

and can be written as

$$\mathbf{F}_{\alpha\beta} = - \left\langle \frac{\partial^2 \ln \mathcal{L}}{\partial \theta_{\alpha} \partial \theta_{\beta}} \right\rangle \Big|_{\boldsymbol{\theta}=\boldsymbol{\theta}_{\text{fid}}}, \quad (3)$$

evaluated at some fixed fiducial parameters. A large Fisher information for a set of data indicates that the data is very informative about the model parameters attributed to it. Fisher forecasting for a given model is made possible by the information inequality and the Cramér-Rao bound (Cramér 1946; Rao 1945), which states that the minimum variance of the value of an estimator $\boldsymbol{\theta}$ is given by

$$\langle (\theta_{\alpha} - \langle \theta_{\alpha} \rangle)(\theta_{\beta} - \langle \theta_{\beta} \rangle) \rangle \geq \mathbf{F}_{\alpha\beta}^{-1}. \quad (4)$$

We will write the compression as a function $f : \mathbf{d} \rightarrow \mathbf{x}$. For large datasets, data compression is essential for inference to avoid the curse of dimensionality. The MOPED

formalism (Heavens et al. 2000) gives optimal score compression for cases where the likelihood and sampling distributions are exactly Gaussian.

IMNNs are neural networks that perform data compression and compute the Fisher information of a data set. Such compression is possible even if the data likelihood is unknown or intractable, simply based on having simulations of the data at a given fiducial parameter point and local information about how the parameters change the data distribution. It can be shown (Wandelt, 2022, in preparation) that the optimality of the IMNN summaries holds for any unknown or intractable data likelihood even though the IMNN maximizes Fisher information assuming the parameter-independent covariance form of the Gaussian likelihood for the IMNN summaries

$$-2 \ln \mathcal{L}(\mathbf{x}|\mathbf{d}) = (\mathbf{x} - \boldsymbol{\mu}_f(\boldsymbol{\theta}))^T \mathbf{C}_f^{-1} (\mathbf{x} - \boldsymbol{\mu}_f(\boldsymbol{\theta})) \quad (5)$$

where

$$\boldsymbol{\mu}_f(\boldsymbol{\theta}) = \frac{1}{n_s} \sum_{i=1}^{n_s} \mathbf{x}_i^s \quad (6)$$

is the mean of the compressed summaries \mathbf{x}_i^s , with $\{\mathbf{x}_i^s | i \in [1, n_s]\}$ and we assume a parameter-independent covariance matrix. Here i indexes the random initialisation of n_s simulations, and the superscript s denotes quantities derived from simulations, unlike quantities without the superscript s which are derived from actual observations. The summaries are obtained via simulation of data $\mathbf{d}_i^s = \mathbf{d}_i^s(\boldsymbol{\theta}, i)$ via the compression scheme $f : \mathbf{d}_i^s \rightarrow \mathbf{x}_i^s$. The covariance of the summaries is computed from the data as well:

$$(\mathbf{C}_f)_{\alpha\beta} = \frac{1}{n_s - 1} \sum_{i=1}^{n_s} (\mathbf{x}_i^s - \boldsymbol{\mu}_f)_{\alpha} (\mathbf{x}_i^s - \boldsymbol{\mu}_f)_{\beta}. \quad (7)$$

Note that this covariance is assumed to be independent of the parameters, which, whilst not strictly true, is enforced by regularisation during the fitting of the IMNN. A Fisher matrix can then be computed from the likelihood in equation (5):

$$\mathbf{F}_{\alpha\beta} = \text{tr}[\boldsymbol{\mu}_{f,\alpha}^T \mathbf{C}_f^{-1} \boldsymbol{\mu}_{f,\beta}], \quad (8)$$

where we introduce the notation $\mathbf{y}_{,\alpha} \equiv \partial \mathbf{y} / \partial \theta_{\alpha}$ for partial derivatives with respect to parameters. If the compression function f is a neural network parameterized by layer weights \mathbf{w}^{ℓ} and biases \mathbf{b}^{ℓ} (with ℓ the layer index), the summaries (and respective mean and covariance) then become functions of these new parameters $\mathbf{x}(\boldsymbol{\theta}) \rightarrow \mathbf{x}(\boldsymbol{\theta}, \mathbf{w}^{\ell}, \mathbf{b}^{\ell})$. To evaluate equation (8) for a neural compression, we must compute

$$\boldsymbol{\mu}_{f,\alpha} = \frac{\partial}{\partial \theta_{\alpha}} \frac{1}{n_s} \sum_{i=1}^{n_s} \mathbf{x}_i^s \text{fid}. \quad (9)$$

One way of computing the derivatives of the summary means with respect to the parameters is to define a finite difference gradient dataset by altering simulation fiducial values by a small amount, yielding

$$\left(\frac{\partial \hat{\mu}_i}{\partial \theta_{\alpha}} \right)^s \text{fid} \approx \frac{1}{n_s} \sum_{i=1}^{n_s} \frac{\mathbf{x}_i^s \text{fid}^{+} - \mathbf{x}_i^s \text{fid}^{-}}{\Delta \theta_{\alpha}^{+} - \Delta \theta_{\alpha}^{-}}. \quad (10)$$

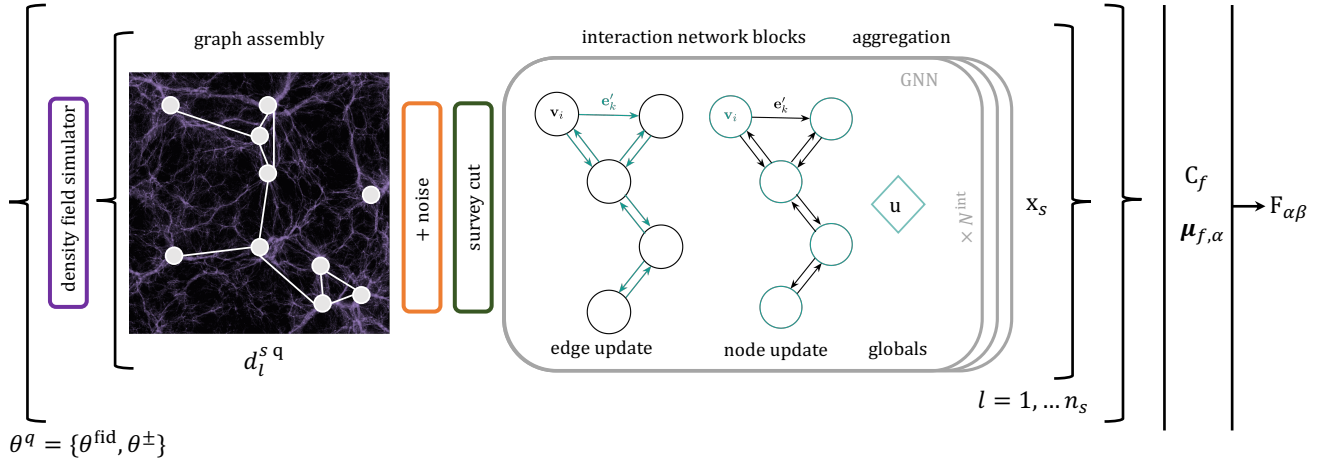


FIG. 2.— Cartoon of the graph-based information maximising neural network scheme. For each $i = 1, \dots, n_s$ dark matter field realization, halo catalogues are computed from a density field and assembled into a connected graph. A GNN block then computes edge and node updates (green) outlined in Section 3.1, pooling graph attributes to compute global summaries, $\mathbf{x} = \mathbf{u}$. This process is repeated for simulations at the fiducial parameter values, as well as at θ^\pm for numerical derivative calculation via equation (10). The output of the IMNN is the Fisher information matrix, computed via equation (8). The network is trained via gradient back-propagation, with the $\det \mathbf{F}$ and \mathbf{C}_f contributing to the scalar loss function.

To prevent extra information being extracted from accidental correlation in limited sized data sets, reported statistics need to be computed on a validation set of simulations, which is unlikely to share the same accidental correlations as the fixed training set. An alternative explored in Makinen et al. (2021) is to calculate the adjoint gradient of the simulations as well as the derivatives of the network parameters with respect to the simulations:

$$\boldsymbol{\mu}_{f,\alpha} = \frac{1}{n_s} \sum_{i=1}^{n_s} \left(\frac{\partial \mathbf{x}}{\partial \theta_\alpha} \right)_i^{s \text{ fid}} = \frac{1}{n_s} \sum_{i=1}^{n_s} \sum_{k=1}^{n_d} \frac{\partial \mathbf{x}_i^{s \text{ fid}}}{\partial d_k} \frac{\partial \mathbf{d}_i^{s \text{ fid}}}{\partial \theta_\alpha}. \quad (11)$$

If the gradient of the simulations can be computed efficiently, this technique for computing the compression Fisher information eliminates the need for hyperparameter tuning of the finite difference derivative size, $\Delta \theta_\alpha$.

The network is trained to maximise the logarithm of the determinant of the Fisher information, computed via equation (8). As described in Charnock et al. and Livet et al., the Fisher information is invariant to nonsingular linear transformations of the summaries. To remove this ambiguity, a term driving covariance to the identity matrix is added

$$\Lambda_C = \frac{1}{2} \left(\left\| (\mathbf{C}_f - \mathbf{1}) \right\|_{\mathcal{F}}^2 + \left\| (\mathbf{C}_f^{-1} - \mathbf{1}) \right\|_{\mathcal{F}}^2 \right), \quad (12)$$

where $\| \mathbf{A} \|_{\mathcal{F}} \equiv \sqrt{\text{tr} \mathbf{A} \mathbf{A}^T}$ denotes the Frobenius norm. This yields the loss function

$$\Lambda = -\ln \det \mathbf{F} + r_{\Lambda_C} \Lambda_C, \quad (13)$$

with regularization parameter

$$r_{\Lambda_C} = \frac{\lambda \Lambda_C}{\Lambda_C + \exp(-\alpha \Lambda_C)}, \quad (14)$$

where λ and α are user-defined parameters. When the covariance is far from identity, the r_{Λ_C} function is large and the optimization focuses on bringing the covariance and its inverse back to identity. The network is trained until the Fisher information stops increasing for a pre-determined number of iterations. We stress that the

value of \mathbf{F} reported as an information metric, however, is the one computed via Eq. 8, computed over a validation set of simulations in the case of a finite set of data.

To summarise the IMNN algorithm we take the following steps *every training epoch* to optimise the Fisher information:

- i) compress simulations at the fiducial model with different random seeds to the network. Calculate the covariance of these summaries using equation (7).
- ii) compress simulations generated at perturbed fiducial parameter values, θ^\pm to produce \mathbf{x}^\pm . Calculate the derivatives $\mathbf{x}_{f,\alpha}$ with equation (10).
- iii) Calculate the Fisher matrix (Eq. (8)). Pass the Fisher and covariance matrices to the loss function. Update neural network weights using gradient descent such that $\det \mathbf{F}$ increases.

3.1. Graph Neural Networks

A graph neural network (GNN) block typically consists of three update functions, $\phi = (\phi_u, \phi_v, \phi_e)$, and three aggregation functions, $\rho = (\rho^u, \rho^v, \rho^e)$, applied sequentially to a graph tuple $G = (\mathbf{u}, V, E)$. A single graph block ℓ is comprised of several update steps to its elements:

1. *Edge update*: Each edge is parameterized by a function $\phi_e^{\ell+1}$ which takes as inputs its connected nodes, previous value, and graph global properties and yields another edge:

$$\mathbf{e}_{ij}^{\ell+1} = \phi_e^{\ell+1}(\mathbf{v}_i^\ell, \mathbf{v}_j^\ell, \mathbf{e}_{ij}^\ell, \mathbf{u}^\ell), \quad (15)$$

where \mathbf{v}_i^ℓ and \mathbf{v}_j^ℓ are sender and receiver nodes indexed by (s_k, r_k) .

2. *Node update*: Each node is then parameterized by a function $\phi_v^{\ell+1}$ and outputs a new node:

$$\mathbf{v}_i^{\ell+1} = \phi_v^{\ell+1}(\rho^{e \rightarrow v}(E_i^{\ell+1}), \mathbf{v}_i^\ell, \mathbf{u}^\ell), \quad (16)$$

Here a permutation-invariant aggregation operation $\rho^{e \rightarrow v}(E_i^{\ell+1})$ pools the neighbourhood of edges

$E_i^{\ell+1}$ connected to node i into a fixed-sized vector to feed into the update function.

3. *Global update*: The global features of the graph are then updated with a function $\phi_u^{\ell+1}$:

$$\mathbf{u}^{\ell+1} = \phi^u(\rho^{e \rightarrow v}(E^{\ell+1}), \rho^{v \rightarrow u}(V^{\ell+1}), \mathbf{u}^\ell), \quad (17)$$

where the graph's edge ($E^{\ell+1}$) and node ($V^{\ell+1}$) sets are pooled into fixed-sized vectors for the global update.

The order of operations of these updates is flexible, but usually applied in the order displayed above, and in the GNN block in Fig. 2. This framework allows ϕ functions to be arbitrarily parameterized as neural networks with nonlinear activation functions. Aggregation functions ρ must be allowed to take a variable number of arguments, so are usually chosen to be permutation-invariant operators such as the mean, summation, or maximum (Bronstein et al. 2021). Stacking $\ell = 1 : N^{\text{int}}$ GNN blocks allows node information to be propagated to and from neighbours N^{int} degrees away, where int refers to *interactions*. In this work all GNN blocks operate over the entire graph. However, one could also devise surrogate GNN blocks that operate on small scales and then pass information up to larger scales via an aggregation function $\rho^{\text{small} \rightarrow \text{large}}$, such that one GNN network is not responsible for operating on nodes of all scales in a densely-populated graph. We detail our specific implementation and architecture in Section 4.1.2.

The GNN framework is readily incorporated into the IMNN formalism, since the details of the neural network architecture only serve to better capture how the data changes with the parameters. Instead of predicting an output graph or class label, as in Battaglia et al. (2018), our final global update ϕ^u outputs IMNN summaries, $\mathbf{x} = \mathbf{u}^{\ell=N^{\text{int}}}$. This new aspect to the IMNN formalism is the ability to operate over variable-length data inputs, rendering the cardinality of input graphs, $n_{\text{data}} = N^v$ and N^e informative features of the data. A stochastic system might yield a different number of discrete particles for different parameters, meaning the *number* of data becomes a descriptor of the statistical model. This allows for a study of information $\mathcal{I} = \frac{1}{2} \ln \det F$ as a function of N^v and enables much more flexible data modelling.

4. COSMOLOGICAL PARAMETER INFERENCE WITH HALO CATALOGUES

Here we consider applications of our graph IMNNs on realistic cosmological problems. Even future astronomical studies will not be able to image complete dark matter overdensity fields of large-scale structure. However, discrete galaxy and void catalogues can be assembled as tracers of structure. Different LSS realizations from stochastic initial conditions will have different numbers of halos and voids, posing a problem for usual fixed-size neural networks, (which are themselves problematic for inference unless treated correctly). We explore information extraction as a function of graph connectivity in the context of two-parameter inference for the matter density parameter, Ω_m , as well as σ_8 , the r.m.s. fluctuation of density perturbations at the $8 \text{ h}^{-1} \text{ Mpc}$ scale. Both Ω_m and σ_8 parameterize the distribution of matter in cosmological simulations, so the graph topology should be sensitive to changes in parameters.

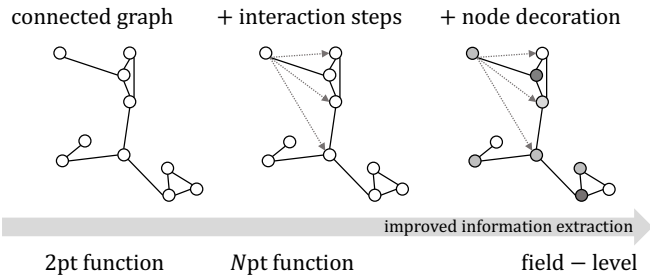


FIG. 3.— Information as a function of large-scale structure data representation. Cosmological parameter information extraction efficiency increases as information is added and propagated throughout the halo graph with increased connections and message-passing steps. The second and third graph show message propagation from the top left node after $N^{\text{int}} = 2$ update steps.

The more descriptive a graph is, the more information one intuitively expects to extract. We demonstrate this trend by first considering *undecorated* graphs, annotated with just positions of and relative distances between halos. We show that information extraction efficiency increases as graph connectivity increases. We then show that information increases further when halo masses are included as node features.

The closest existing statistics to this representation are n -point correlation and mass functions, and we show how information increases beyond the 2-point correlation function with the same catalogue as graph connectivity is increased, as illustrated in the cartoon in Figure 3.

4.1. Halo Catalogues

Here we describe the simulated catalogues that are used for training and validation. The Quijote Halo catalogues are assembled from 3D overdensity fields at the present day ($z = 0$) using the Friends of Friends (FoF) algorithm (Davis et al. 1985). Attributes computed by the finder are halo masses M_i , positions \mathbf{p}_i , and velocities \mathbf{v}_i . Each full simulation yields a catalogue of $\sim 400,000$ halos on average. Here we restrict our analysis to mass and clustering information in an effort to compare our method to known statistics.

4.1.1. Graph inputs assembly

We initially connect graphs of a manageable size by varying two hyperparameters. We first make a minimum mass cut M_{cut} to be considered in the catalogue. Nodes are then connected to one another within a Euclidean distance r_{connect} . We initially explore the noise-free limit with known masses and fix $M_{\text{cut}} = 1.5 \times 10^{15} M_\odot$ to assess the pure information limit of the catalogues. We add noise to the analysis in Section 6. This cut yields $N^v \in [70, 140]$ halos per catalogue. We visualize two graphs in Appendix B, figure 2.

We then assemble the truncated catalogues into non-invariant and invariant graphs, as outlined in Section 2.2. We initialize each graph's global property with a tuple $\mathbf{u}^{\ell=0} = (\text{arcsinh } N^v, \text{arcsinh } N^e)$ summarising the cardinality of the graphs. As described in Battaglia et al. (2018); Lemos et al. (2022); Villanueva-Domingo & Villaescusa-Navarro (2022), imposing symmetries in data representation can improve GNN training, since the network can focus on learning relevant correlations to the problem, as opposed to re-learning symmetry. We test this notion in the context of information extraction.

4.1.2. Graph neural network architecture

We choose to parameterize our GNN functions with simple fully-connected networks. Each ϕ function is a dense network with two layers of 50 hidden neurons and `gelu` activations (Hendrycks & Gimpel 2016). We built a custom aggregation function akin to that found in Villanueva-Domingo & Villaescusa-Navarro (2022), in which mean, max, sum, and variance are computed over node and edge attributes and then concatenated, since it is not known a priori which function is most useful for information extraction. To aggregate e.g. the set of edges E_i in a neighbourhood around node i we compute:

$$\bigoplus_{j \in E_i} \mathbf{e}_{ij} = \left[\max_{j \in E_i} \mathbf{e}_{ij}, \sum_{j \in E_i} \mathbf{e}_{ij}, \frac{\sum_{j \in E_i} \mathbf{e}_{ij}}{\sum_{j \in E_i} 1} \right] \quad (18)$$

We additionally modify these operators with a trainable `arcsinh` layer e.g. for edge-to-node aggregation:

$$\rho_{e \rightarrow v}^{\ell+1}(E_i^\ell) = a \operatorname{arcsinh} \left(b \bigoplus_{j \in E_i^\ell} \mathbf{e}_{ij}^\ell + c \right) + d, \quad (19)$$

where (a, b, c, d) are scalar learnable parameters initialized as $(1, 1, 0, 0)$ to ensure numerical stability for gradient calculation. All networks are trained with an Adam optimizer with a learning rate set to 0.0001 and coupling parameters $\lambda = 10$ and $\alpha = 0.95$. We construct our graphs and GNNs using the `jraph` (Godwin et al. 2020) and `Flax` (Heek et al. 2020) libraries, which are both `Jax`-compatible.

We train our gIMNNs by splitting the *Quijote* simulations into equally-sized training and validation sets. Gradient descent is performed on training data, while reported compression statistics (Fisher information) are computed for the *validation* set using equation (8). Both training and validation sets comprise of $n_s = 500$ fiducial simulations at $\theta_{\text{fid}} = (\Omega_m, \sigma_8) = (0.3175, 0.834)$ and $n_d = 250$ seed-matched derivative simulations perturbed by $\delta\theta = (0.01, 0.015)$, yielding $n_d \times 2 \times 2 = 1000$ simulations (see Villaescusa-Navarro et al. (2020b) for details). Training on the loss defined in Eq 13 is performed until a patience criterion is met, in this case, when the training Fisher information stops increasing significantly for 1000 epochs.

4.2. Undecorated Graphs vs. n -point Statistics

We first consider an undecorated graph representation of halo catalogues *without* descriptive node features. Drawing more edges between nodes increases the connectivity of the graph, allowing information from a single node to reach more distant neighbours. Undecorated graphs of increasing connectivity are analogous to traditional n -point statistics computed for galaxy catalogues. 3-point statistics for example consider triangular groupings of galaxies, and generally offer tighter constraints from large-scale structure data than the 2PCF, as shown in (Hahn et al. 2020). We additionally explore invariant and non-invariant graph structures, outlined in Section 2.2.

4.2.1. Comparison to 2-point correlation information

As a benchmark for our analysis, we also compare the information content obtained from the 2-point correlation function (2PCF), $\xi(r)$, of our small halo catalogues, the real-space equivalent to the *Quijote* power spectrum computed in Villaescusa-Navarro et al. (2020b). For a statistic $Q = \xi(r)$, the Fisher information is given by (Tegmark et al. 1997):

$$F_{ij} = \frac{1}{2} \operatorname{tr} \left\{ \mathbf{C}^{-1} \left[\left(\frac{\partial Q}{\partial \theta_i} \frac{\partial Q}{\partial \theta_j} \right) + \left(\frac{\partial Q}{\partial \theta_i} \frac{\partial Q}{\partial \theta_j} \right)^T \right] \right\}, \quad (20)$$

where \mathbf{C} is estimated from simulations at the fiducial and the derivatives are approximated numerically via

$$\frac{\partial Q}{\partial \theta_i} \approx \frac{Q(\theta_i^+) - Q(\theta_i^-)}{\theta_i^+ - \theta_i^-} \quad (21)$$

We use the full suite of 500 derivative and 1000 fiducial halo catalogue simulations to compute Eq 20, and crucially *make the same conservative mass cut*. We bin distances into 10 fixed bins between 0 and $\sqrt[3]{3}$ Gpc³, yielding a covariance matrix of size 100². For the 2PCF we obtain a Fisher information of 2.28×10^6 , or Shannon entropy of 7.319 nats.

4.2.2. Increasing graph connectivity

Here we construct graphs of varying edge cardinality by varying a physical connection parameter, $r_{\text{connect}} \in \{100, 200, 300\}$ Mpc, yielding graphs with average edge number $\langle N^e \rangle \in \{27, 150, 437\}$ respectively. We also compare information as a function of increasing GNN interaction blocks, N^{int} , for all r_{connect} , for both non-invariant and invariantly-structured halo graphs. Network architecture is identical for each r_{connect} value, and initialized by the same random seed.

Results. We display information extraction as a function of graph connectivity in Figure 4, computed for the validation simulation set. We also display the catalogue’s 2PCF information (dashed line) as a benchmark. Invariant graphs (top row) train more smoothly than non-invariant graphs (bottom row) since the network does not have to learn relationships from position values on the nodes. A single GNN block struggles to extract information with $r_{\text{connect}} = 100$ Mpc in the non-invariant representation (lower left), but plateaus at $\approx 2.8 \times 10^7$ for all other configurations. This behavior is likely because in most cases the network is both descriptive enough and is able to capture patterns at much larger scales by attending to halos higher degrees away. The common saturation value across multiple network and connectivity combinations indicates that undecorated graphs typically contain $\det F_{\text{IMNN}} / \det F_{2\text{PCF}} \approx 10 - 15$ times more information than the 2PCF, regardless of connectedness, provided a descriptive enough network can extract it. The graph representation improves marginal constraints in Ω_m by a factor of ≈ 2 and in σ_8 by a factor of ≈ 11 , displayed in Figure 5.

We initially hypothesized that increasing network complexity would increase the information extraction. However, we found that we obtain essentially equivalent information for any combination of r_{connect} and N^{int} . It is clear that for this small number of halos the informa-

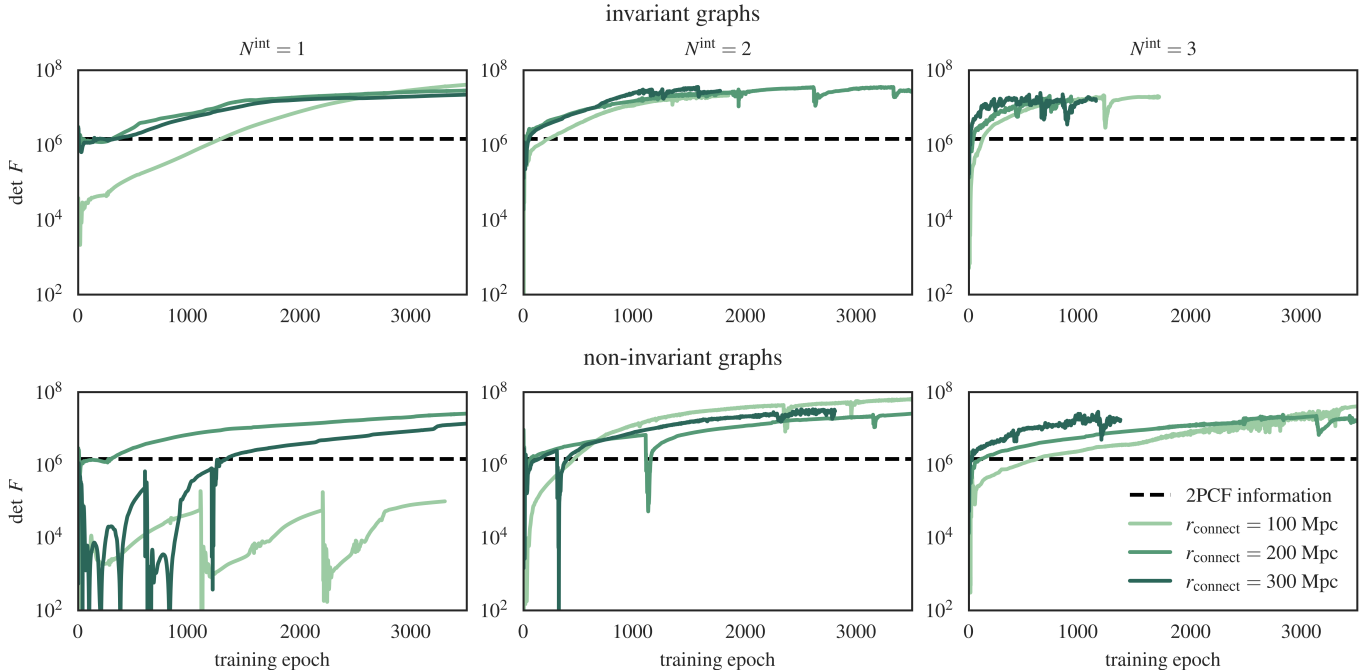


FIG. 4.— Information extraction comparison for undecorated invariant (*top row*) and non-invariant (*bottom row*) halo graphs over validation simulations. Columns indicate how many graph network update steps are performed, and colours indicate graphs assembled with different physical connection radii. The information obtained from the 2PCF computed from the same catalogues with the same mass cut is shown as a dashed line. For sufficiently descriptive networks ($N^{\text{int}} > 1$), invariantly-assembled graphs train faster, but all graphs connected for $r > 100$ Mpc saturate at $\det F \approx 2.8 \times 10^7$, or ≈ 15 times higher than the 2PCF. Jagged dips in validation curves indicate points of restarting network training after patience criteria were met.

tion is easily saturated at any level, but with more halos in the catalogue, as discussed in Section 8, hierarchical clustering at the graph or network level might pull out more information from e.g. smaller mass scales. This exploration is reserved for a future work.

Since all sufficiently-connected representations obtain the same information, we proceed in our experiments with invariant graphs connected with $r_{\text{connect}} = 200$ Mpc and $N^{\text{int}} = 2$, since this combination resulted in the smoothest and fastest training (4 minutes) on a single NVIDIA-v100 GPU.

4.3. Decorated Graphs: Incorporating Halo Mass

We next decorate each halo node with the corresponding (noise-free) halo mass. We widen the network’s hidden dimension to 64 and train both decorated and undecorated graphs with the same patience settings. Training was restarted for each three times after plateau to ensure saturation. The same network architecture is able to extract 2.3 times more information when decorated with masses, corresponding to 42 times more information than the 2PCF. We display the corresponding Fisher ellipses in Figure 5, along with isomass lines of the halo mass function, described in Section 5.1. We also decorated graphs with peculiar velocities with slight improvement in information extraction but restricted our analysis to mass and clustering for interpretability.

5. MASS CUT INFORMATION

We next investigate how much information is contained in the mass cut, M_{cut} which determines halo number N^v . We compare two graph assemblies: one with a *fixed* number of the most massive halos $N_{\text{fixed}}^v = 105$, i.e. the

average number of halos across variable sized halo catalogues with fixed mass cut $M_{\text{cut}} = 1.5 \times 10^{15} M_{\odot}$, and another where the cardinality is allowed to vary with M_{cut} . For each case we compare decorated and undecorated graphs, and the network (epistemic) and data sampling (aleatoric) errors associated with each representation. To

catalogue N^v	graph assembly	$\ln \det F$	vary network	vary data
fixed	without mass		5.03 ± 0.47	5.98 ± 1.06
	with mass		12.43 ± 1.44	12.39 ± 0.22
	2PCF	9.74		
variable	without mass		17.89 ± 0.33	17.66 ± 0.27
	with mass		17.40 ± 0.57	17.85 ± 0.12
	2PCF	14.19		

TABLE 1

Comparison of extracted information from fixed- and variable-length catalogues. Information was extracted with $r_{\text{connect}} = 200$ Mpc, and networks with $N^{\text{int}} = 2$ across 5 identical initializations. We display each configuration’s best Fisher information and the means and standard deviations over 5 network initializations (second-to-last column) and 5 different train/validation set splits (last column).

estimate network variability we train five gIMNNs with $N^{\text{int}} = 2$ with different initialization of network parameters, whilst fixing the training and validation sets, displaying the best Fisher obtained as well as the mean and standard deviation of $\ln \det F$ over the five runs. For data sampling uncertainty we fix the gIMNN weight values on initialization and train on five different randomised train-validation equal-sized splits of the available simulations. For both data and network error cases, the same five random seeds and network architecture is used across all

data configurations.

Results. We display results in Table 1. Fixing catalogue size eliminates halo number as a useful feature to the network, evidenced by much lower information yields. Without mass decoration there is less information in the graph data so the data can be fit by more possible functions by the network, so the variability of the Fisher as a function of the data sampling is increased over the decorated case. However, the network has to fit a simpler compression since there are fewer relevant features without mass, so the variability in possible network weights decreases, compared to the decorated case. Fixed-length graphs do not exceed the 2PCF information until annotated with mass information.

When catalogues are allowed to vary with a physical mass cut, much more information can be extracted from both decorated and undecorated graphs. Including mass information on the nodes again increases the variability incurred across different network initializations, but decreases the aleatoric uncertainty since we better describe the likelihood with more information.

5.1. Comparison to the Halo Mass Function

The results of Section 5 indicate that catalogue information extraction is extremely sensitive to a physical mass cut. This behaviour is akin to constraints obtained using halo mass cumulative distribution functions (Reed et al. 2006; Uhlemann et al. 2020; Artis et al. 2021). The halo number density function is dn/dM , defined as the number of halos of mass M per unit volume per unit interval in M , equivalently parameterized using the smoothed r.m.s. linear overdensity of the density field, $\sigma(M)$, via the halo mass function (HMF), $f(\sigma)$. The fraction of mass in collapsed halos per unit interval $\ln \sigma^{-1}$ obeys

$$\int_{-\infty}^{\infty} f(\sigma) d \ln \sigma^{-1} = 1, \quad (22)$$

and is related to the halo number density function via

$$\frac{dn}{dM} = \frac{\rho_o}{M} \frac{d \ln \sigma^{-1}}{dM} f(\sigma), \quad (23)$$

where ρ_o is the mean mass density of the universe. The form of $f(\sigma; \theta)$ can be related analytically to cosmological parameters, such as in Press & Schechter (1974), or approximated using simulations (Reed et al. 2006).

We compare gIMNN Fisher constraints to iso-mass contours of the integrated Press-Schechter HMF, $f_{\text{PS}}(\sigma; \Omega_m, \sigma_8)$, integrated from a fixed M_{cut} as a function of cosmological parameters in Figure 5. We use the HMF since this quantity incorporates both halo number and mass information. See Appendix A for a detailed comparison of dn/dM and $f(\sigma)$ functions. We utilize `hmf calc` (Murray et al. 2013; Murray 2014) for the calculation. The HMF and the corresponding halo number density at fixed $M = M_{\text{cut}}$ determines a

relatively narrow locus in the (Ω_m, σ_8) plane. The clustering information, traced by the 2PCF Fisher, (which is accessible by the network) serves to lift this degeneracy. The network Fishers are nearly parallel to the HMF iso-mass contours, but are not degenerate in the direction of the 2PCF Fisher’s major axes. Decorating nodes with masses also induces a slight rotation towards the isomass contours, since the network has more detailed mass information to work with. This result indicates that *the*

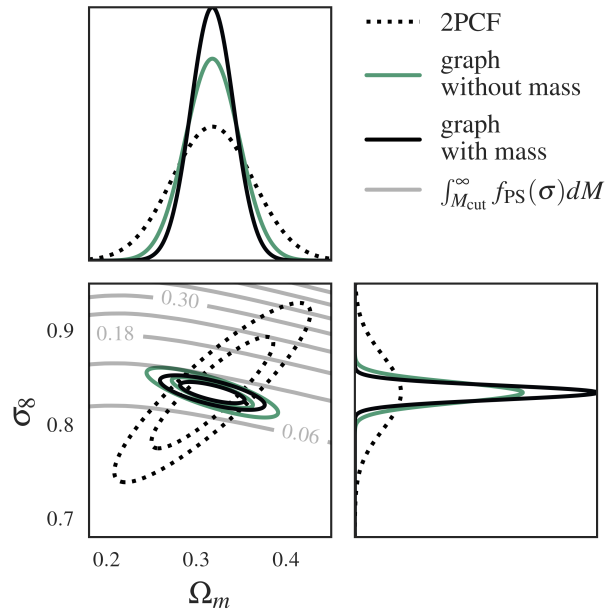


FIG. 5.— Fisher matrix comparison for decorated (black) and undecorated (green) graphs and 2PCF (dashed) computed for the same catalogue, plotted over contours of the Press-Schechter halo mass function (grey), where the numbers indicate the integrated mass density of halos from M_{cut} to infinity, as a function of Ω_m and σ_8 . The HMF contours indicate the information provided by a fixed physical mass cut, orthogonal to the positional information in the 2PCF. The IMNN Fisher ellipses follow these contours, but are not degenerate in the direction of the 2PCF, indicating that the IMNN has learned to use both mass and clustering information. Graphs annotated with halo mass tighten constraints by a factor of 2.3 over undecorated graphs, and by a factor of 42 over 2PCF information.

network has automatically learned to extract information from both halo clustering and mass information.

6. WORKING WITH NOISY CATALOGUES

We next add observational noise and catalogue cuts on-the-fly during gIMNN training to mimic survey assembly with imperfect observations. Before a graph is constructed from a halo catalogue and fed to the network in training, halo masses are subjected to white noise with fixed variance,

$$\hat{m}_i = m_i + \mathcal{N}(0, \sigma_{\text{noise}}^2), \quad (24)$$

where $\sigma_{\text{noise}} = A_{\text{noise}} M_{\text{cut}}$. Observed halos that fall below M_{cut} are then trimmed from the graph to mimic real catalogue cuts in the presence of noisy mass estimates. This noise model reflects uncertainty in the halo finder or galaxy catalogue builder. Smaller masses close to M_{cut} are more likely to be cut due to mass underestimation, similar to low-brightness clusters in sky surveys. We choose $M_{\text{cut}} = 1.5 \times 10^{15} M_{\odot}$ and train identical networks with different amplitudes of on-the-fly noise; $A_{\text{noise}} \in \{0.05, 0.1, 0.2\}$.

Results. We display validation curves over training epoch in Figure 6. Increasing catalogue noise results in higher variance per epoch in the computed Fisher statistics, as well as a slightly lower information plateau. This can be interpreted as higher noise obscuring small mass scales in the information extraction. This effect is illustrated via inflated Fisher constraints in Figure 7.

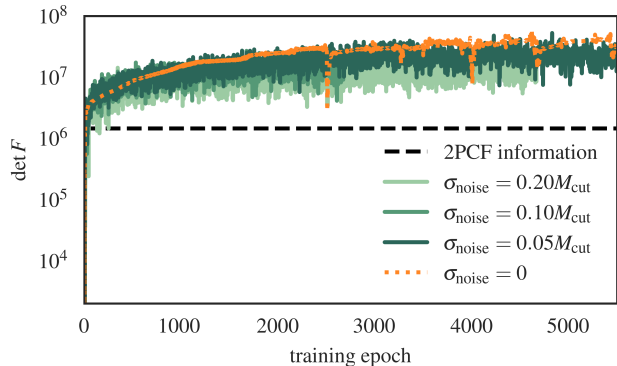


FIG. 6.— Validation curves for noisy masses. Smaller noise variance (darker curves) results in smaller per-epoch variance in $\det F$ and slightly more information extraction. Information leakage occurs with higher noise variance since smaller scales are poorly resolved and trimmed from the catalogue.

As the noise level increases the low-end masses have more variance when drawn on-the-fly so more halos are projected out of the catalogue because they fall below M_{cut} , and so this information cannot be encapsulated in the compressed summaries. Increasing the noise amplitude to 20% of M_{cut} inflates constraints in Ω_m . In the high-noise limit, halo positions dominate $\det F$, indicated by the relatively unchanged, position-dependent σ_8 constraints. As noise decreases and masses are better known, the Fisher exhibits the same rotation seen in Section 5.1 along the isomass HMF lines. This effect is discussed in detail in Appendix A.

Despite inflating constraints, showing the network large numbers of on-the-fly noise realizations during training can harden the network to the negative effects of limited training data and therefore provide smoother training whilst still being able to extract information at a similar level to noise-free catalogues. However, the model of these noisy masses must be accurate to the noise model expected for the real data otherwise the on-the-fly simulations do not provide hardening of the summaries in the correct way and may even project out informative data correlations.

7. APPLICATION TO IMPLICIT LIKELIHOOD INFERENCE

The IMNN framework is both an information quantification scheme as well as an asymptotically optimal compression mechanism for implicit likelihood inference. The global network summaries used to compute Fisher statistics can also be used as proxies for the cosmological parameters via a score estimate (Alsing & Wandelt 2018; Charnock et al. 2018) using the IMNN Fisher and covariance:

$$\hat{\theta}_\alpha = \mathbf{F}_{\alpha\beta}^{-1} \frac{\partial \mu_i}{\partial \theta_\beta} \mathbf{C}_{ij}^{-1} (x_j(\mathbf{w}, \mathbf{d}) - \mu_j). \quad (25)$$

These summaries are *not* explicit predictions for cosmological parameters, although they are pseudo-maximum likelihood estimates for the parameters in the region asymptotically close to the fiducial cosmological parameter values. Instead, we suggest using these values as informative summaries in Approximate Bayesian Computation (ABC) or density estimation schemes, as demonstrated in Makinen et al. (2021) and Charnock et al. (2018). Figure 8 shows a spread of these summaries

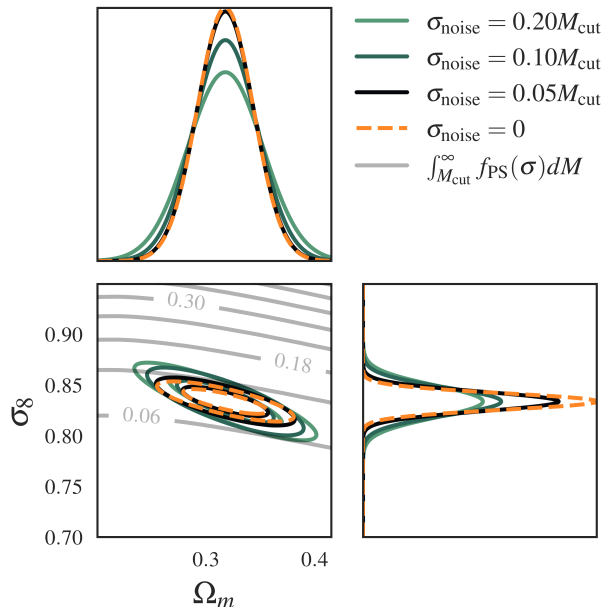


FIG. 7.— Fisher constraints for different noise models, plotted over lines of the Press-Schechter halo mass function integrated from M_{cut} (grey), where the numbers indicate the integrated mass density of halos from M_{cut} to infinity, as a function of Ω_m and σ_8 . Higher σ_{noise} (lighter curves) cause low-mass halos to drop out, inflating constraints in Ω_m , but constraints in σ_8 remain relatively unchanged since this parameter is largely position-dependent.

over 200 test (non-seed matched with cosmic variance) θ^\pm Quijote datasets. The network is able to distinguish halo graphs simulated at different parameter values (on the level of the parameter degeneracy), rendering these gIMNN summaries usable in accept-reject simulation-based inference (SBI) schemes. We additionally discuss network generalization to other data in Appendix B.

8. DISCUSSION & CONCLUSION

In this study, we explored cosmological information extraction from halo catalogues assembled as graphs. We first introduced graphs as a general language for describing large-scale structure formation. We showed that nonlinear summaries from sufficiently expressive graph neural networks far exceed the information contained in traditional 2-point statistics, using the ≈ 100 most massive halos. We illustrated that decorating graphs with mass information increases the information yield, as well as decreases training-validation set sampling variance (aleatoric error). Finally, we showed that summaries produced by the network are readily usable for simulation-based inference.

We also explored cosmological information as a function of graph construction. We showed that a significant amount of information is contained in the variable cardinality of the graph, N^v , i.e. the number of halos in a catalogue, and related this feature to the halo mass function formalism. This test demonstrated a distinct advantage in graph representation: allowing data vector size to vary with cosmology, *combining both positional and mass information automatically into just two statistics*.

Next we demonstrated that gIMNN training can be made robust to noise with little information loss in a

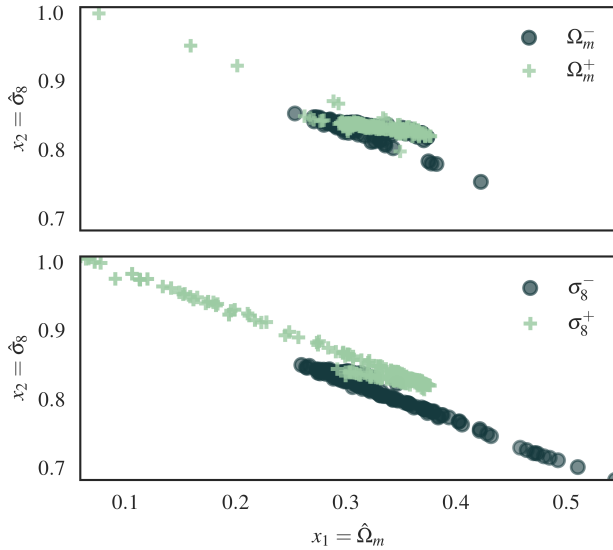


FIG. 8.— gIMNN score summaries for test derivative datasets (θ^\pm with cosmic variance). A trained network can distinguish between simulations generated at different parameter values, indicated by the different distributions in summary space. These score summaries are *not* explicit predictions for cosmological parameters; they should be considered as informative summaries of the cosmological parameters that can be used for ABC or density estimation for building cosmological posteriors. In general and on average, simulations generated at lower Ω_m and σ_8 values have lower pseudo-maximum likelihood estimated values for these parameters and vice versa, however, they should not be taken as predictions of the cosmological parameters.

more realistic setting where halo masses are estimates with measurement error.

We also explored network (epistemic) and data sampling (aleatoric) error in graph representation. We showed that a combined compression of masses and positional information *decreased* data variability, meaning training and validation graphs become more descriptive of their underlying likelihood with decoration, even in a fixed-length scenario.

The results of this work hold several implications for cosmological parameter estimation and study of large-scale structure. The graph framework presented here enables further modular study of nonlinear statistics that combine attributes of mass functions and correlation functions, at a fraction of the computational cost of bispectrum or trispectrum calculation. Cosmological

parameter constraints from void catalogues, here the duals to halo graphs, might elucidate complementary constraints to those obtained here (Kreisch et al. 2021).

Coulton et al. (2022) and Jung et al. (2022) recently investigated bispectrum statistics from n-body primordial nongaussianity (pNG) simulations in the *Quijote* suite to investigate propagation of pNG to late-time cosmological structure. A complementary study using gIMNNs might pick up signatures not isolated in the bispectrum framework. The gIMNN formalism could also be used to summarise and understand better the halo merger and clustering statistics as a function of scale or graph feature, such as clique number. Hierarchical aggregation schemes, as described in Section 3.1, could make the gIMNN scheme tractable for aggregating catalogued galaxies into subhalo graphs, and further into a global graph over the largest scales. Doing so would scale this analysis to full-sized galaxy catalogues.

Follow-up study is warranted on much larger catalogues and with more parameters, with a view to readying this framework for applications to inference from detailed physical simulations and, ultimately, realistic galaxy surveys.

9. CODE AVAILABILITY

The code used for this analysis is available at <https://github.com/tlmakinen/cosmicGraphs>. Full documentation for the IMNN software is available at <https://www.aquila-consortium.org/doc/imnn/index.html>.

T.L.M acknowledges the Imperial College London President’s Scholarship fund for support of this study, as well as the great discussions with Stephon Alexander, David Spergel, and Doug Finkbeiner that inspired this work. B.D.W. acknowledges support by the ANR BIG4 project, grant ANR-16-CE23-0002 of the French Agence Nationale de la Recherche; and the Labex ILP (reference ANR-10-LABX-63) part of the IDEX SUPER, and received financial state aid managed by the Agence Nationale de la Recherche, as part of the programme Investissements d’avenir under the reference ANR-11-IDEX-0004-02. This work was done within the *Aquila Consortium* and the *Learning the Universe Collaboration*. The Flatiron Institute is supported by the Simons Foundation.

REFERENCES

- Adami, C., & Mazure, A. 1999, *Astron. Astrophys. Suppl. Ser.*, 134, 393, doi: [10.1051/aas:1999145](https://doi.org/10.1051/aas:1999145)
- Alpaslan, M., Robotham, A. S. G., Driver, S., et al. 2014, *MNRAS*, 438, 177, doi: [10.1093/mnras/stt2136](https://doi.org/10.1093/mnras/stt2136)
- Alsing, J., & Wandelt, B. 2018, *MNRAS*, 476, L60, doi: [10.1093/mnrasl/sly029](https://doi.org/10.1093/mnrasl/sly029)
- Artis, E., Melin, J.-B., Bartlett, J. G., & Murray, C. 2021, *Astronomy & Astrophysics*, 649, A47, doi: [10.1051/0004-6361/202140293](https://doi.org/10.1051/0004-6361/202140293)
- Barrow, J. D., Bhavsar, S. P., & Sonoda, D. H. 1985, *Monthly Notices of the Royal Astronomical Society*, 216, 17, doi: [10.1093/mnras/216.1.17](https://doi.org/10.1093/mnras/216.1.17)
- Battaglia, P. W., Hamrick, J. B., Bapst, V., et al. 2018, *Relational inductive biases, deep learning, and graph networks*. <https://arxiv.org/abs/1806.01261>
- Beuret, M., Billot, N., Cambr esy, L., et al. 2017, *A&A*, 597, A114, doi: [10.1051/0004-6361/201629199](https://doi.org/10.1051/0004-6361/201629199)
- Bhavsar, S. P., & Ling, E. N. 1988, *PASP*, 100, 1314, doi: [10.1086/132325](https://doi.org/10.1086/132325)
- Biswas, R., Alizadeh, E., & Wandelt, B. D. 2010, *Phys. Rev. D*, 82, 023002, doi: [10.1103/PhysRevD.82.023002](https://doi.org/10.1103/PhysRevD.82.023002)
- Bonnaire, T., Aghanim, N., Decelle, A., & Douspis, M. 2020, *Astronomy & Astrophysics*, 637, A18, doi: [10.1051/0004-6361/201936859](https://doi.org/10.1051/0004-6361/201936859)
- Bonnaire, T., Aghanim, N., Kuruvilla, J., & Decelle, A. 2022, *Astronomy & Astrophysics*, 661, A146, doi: [10.1051/0004-6361/202142852](https://doi.org/10.1051/0004-6361/202142852)
- Bronstein, M. M., Bruna, J., Cohen, T., & Veličković, P. 2021, *Geometric Deep Learning: Grids, Groups, Graphs, Geodesics, and Gauges*, arXiv, doi: [10.48550/ARXIV.2104.13478](https://doi.org/10.48550/ARXIV.2104.13478)
- Charnock, T., Lavaux, G., & Wandelt, B. D. 2018, *Physical Review D*, 97, doi: [10.1103/physrevd.97.083004](https://doi.org/10.1103/physrevd.97.083004)
- Colberg, J. M. 2007, *Monthly Notices of the Royal Astronomical Society*, 375, 337, doi: [10.1111/j.1365-2966.2006.11312.x](https://doi.org/10.1111/j.1365-2966.2006.11312.x)

- Coles, P., Pearson, R. C., Borgani, S., Plionis, M., & Moscardini, L. 1998, *MNRAS*, 294, 245, doi: [10.1046/j.1365-8711.1998.01147.x](https://doi.org/10.1046/j.1365-8711.1998.01147.x)
- Coulton, W. R., Villaescusa-Navarro, F., Jamieson, D., et al. 2022, Quijote-PNG: Simulations of primordial non-Gaussianity and the information content of the matter field power spectrum and bispectrum, arXiv, doi: [10.48550/ARXIV.2206.01619](https://doi.org/10.48550/ARXIV.2206.01619)
- Cramer, H. 1946, *Mathematical methods of statistics*, by Harald Cramer, .. (The University Press)
- Crammer, M., Sanchez-Gonzalez, A., Battaglia, P., et al. 2020, Discovering Symbolic Models from Deep Learning with Inductive Biases. <https://arxiv.org/abs/2006.11287>
- Dai, B., & Seljak, U. 2022, arXiv e-prints, arXiv:2202.05282. <https://arxiv.org/abs/2202.05282>
- Davis, M., Efstathiou, G., Frenk, C. S., & White, S. D. M. 1985, *ApJ*, 292, 371, doi: [10.1086/163168](https://doi.org/10.1086/163168)
- Fluri, J., Kacprzak, T., Lucchi, A., et al. 2019, *Physical Review D*, 100, doi: [10.1103/physrevd.100.063514](https://doi.org/10.1103/physrevd.100.063514)
- Fluri, J., Kacprzak, T., Lucchi, A., et al. 2022, arXiv e-prints, arXiv:2201.07771. <https://arxiv.org/abs/2201.07771>
- Fluri, J., Kacprzak, T., Refregier, A., et al. 2018, *Physical Review D*, 98, doi: [10.1103/physrevd.98.123518](https://doi.org/10.1103/physrevd.98.123518)
- Fluri, J., Kacprzak, T., Refregier, A., Lucchi, A., & Hofmann, T. 2021, *Physical Review D*, 104, doi: [10.1103/physrevd.104.123526](https://doi.org/10.1103/physrevd.104.123526)
- Gillet, N., Mesinger, A., Greig, B., Liu, A., & Ucci, G. 2019, Monthly Notices of the Royal Astronomical Society, doi: [10.1093/mnras/stz010](https://doi.org/10.1093/mnras/stz010)
- Godwin, J., Keck, T., Battaglia, P., et al. 2020, Jraph: A library for graph neural networks in jax, 0.0.1.dev. <http://github.com/deepmind/jraph>
- Hahn, C., Villaescusa-Navarro, F., Castorina, E., & Scoccimarro, R. 2020, *Journal of Cosmology and Astroparticle Physics*, 2020, 040, doi: [10.1088/1475-7516/2020/03/040](https://doi.org/10.1088/1475-7516/2020/03/040)
- Hamaus, N., Sutter, P., Lavaux, G., & Wandelt, B. D. 2015, *Journal of Cosmology and Astroparticle Physics*, 2015, 036–036, doi: [10.1088/1475-7516/2015/11/036](https://doi.org/10.1088/1475-7516/2015/11/036)
- Heavens, A. F., Jimenez, R., & Lahav, O. 2000, Monthly Notices of the Royal Astronomical Society, 317, 965–972, doi: [10.1046/j.1365-8711.2000.03692.x](https://doi.org/10.1046/j.1365-8711.2000.03692.x)
- Heek, J., Levsakaya, A., Oliver, A., et al. 2020, Flax: A neural network library and ecosystem for JAX, 0.5.2. <http://github.com/google/flax>
- Hendrycks, D., & Gimpel, K. 2016, Gaussian Error Linear Units (GELUs), arXiv, doi: [10.48550/ARXIV.1606.08415](https://doi.org/10.48550/ARXIV.1606.08415)
- Jamieson, D., Li, Y., de Oliveira, R. A., et al. 2022, Field Level Neural Network Emulator for Cosmological N-body Simulations, arXiv, doi: [10.48550/ARXIV.2206.04594](https://doi.org/10.48550/ARXIV.2206.04594)
- Jasche, J., Leclercq, F., & Wandelt, B. 2015, *Journal of Cosmology and Astroparticle Physics*, 2015, 036, doi: [10.1088/1475-7516/2015/01/036](https://doi.org/10.1088/1475-7516/2015/01/036)
- Jasche, J., & Wandelt, B. D. 2013, *MNRAS*, 432, 894, doi: [10.1093/mnras/stt449](https://doi.org/10.1093/mnras/stt449)
- Jeffrey, N., Alsing, J., & Lanusse, F. 2020, Monthly Notices of the Royal Astronomical Society, 501, 954, doi: [10.1093/mnras/staa3594](https://doi.org/10.1093/mnras/staa3594)
- Jeffrey, N., Boulanger, F., Wandelt, B. D., et al. 2022, *MNRAS*, 510, L1, doi: [10.1093/mnras/lsab120](https://doi.org/10.1093/mnras/lsab120)
- Jeffrey, N., & Wandelt, B. D. 2020, Solving high-dimensional parameter inference: marginal posterior densities & Moment Networks. <https://arxiv.org/abs/2011.05991>
- Jung, G., Karagiannis, D., Liguori, M., et al. 2022, Quijote-PNG: Quasi-maximum likelihood estimation of Primordial Non-Gaussianity in the non-linear dark matter density field, arXiv, doi: [10.48550/ARXIV.2206.01624](https://doi.org/10.48550/ARXIV.2206.01624)
- Kipf, T. N., & Welling, M. 2016, Semi-Supervised Classification with Graph Convolutional Networks, arXiv, doi: [10.48550/ARXIV.1609.02907](https://doi.org/10.48550/ARXIV.1609.02907)
- Kreisch, C. D., Pisani, A., Villaescusa-Navarro, F., et al. 2021, The GIGANTES dataset: precision cosmology from voids in the machine learning era, arXiv, doi: [10.48550/ARXIV.2107.02304](https://doi.org/10.48550/ARXIV.2107.02304)
- Krzewina, L. G., & Saslaw, W. C. 1996, *MNRAS*, 278, 869, doi: [10.1093/mnras/278.3.869](https://doi.org/10.1093/mnras/278.3.869)
- Kwon, Y., Hong, S. E., & Park, I. 2020, *Journal of the Korean Physical Society*, 77, 49–59, doi: [10.3938/jkps.77.49](https://doi.org/10.3938/jkps.77.49)
- Lavaux, G., & Wandelt, B. D. 2010, *MNRAS*, 403, 1392, doi: [10.1111/j.1365-2966.2010.16197.x](https://doi.org/10.1111/j.1365-2966.2010.16197.x)
- Leclercq, F. 2015, Bayesian large-scale structure inference and cosmic web analysis, arXiv, doi: [10.48550/ARXIV.1512.04985](https://doi.org/10.48550/ARXIV.1512.04985)
- Leclercq, F., & Heavens, A. 2021, On the accuracy and precision of correlation functions and field-level inference in cosmology. <https://arxiv.org/abs/2103.04158>
- Lemos, P., Jeffrey, N., Cranmer, M., Ho, S., & Battaglia, P. 2022, Rediscovering orbital mechanics with machine learning. <https://arxiv.org/abs/2202.02306>
- Libeskind, N. L., van de Weygaert, R., Cautun, M., et al. 2018, *MNRAS*, 473, 1195, doi: [10.1093/mnras/stx1976](https://doi.org/10.1093/mnras/stx1976)
- Livet, F., Charnock, T., Borgne, D. L., & de Lapparent, V. 2021, Catalog-free modeling of galaxy types in deep images: Massive dimensional reduction with neural networks. <https://arxiv.org/abs/2102.01086>
- Makinen, T. L., Charnock, T., Alsing, J., & Wandelt, B. D. 2021, *Journal of Cosmology and Astroparticle Physics*, 2021, 049, doi: [10.1088/1475-7516/2021/11/049](https://doi.org/10.1088/1475-7516/2021/11/049)
- Makinen, T. L., Lancaster, L., Villaescusa-Navarro, F., et al. 2020, deep21: a Deep Learning Method for 21cm Foreground Removal. <https://arxiv.org/abs/2010.15843>
- Massara, E., Villaescusa-Navarro, F., Hahn, C., et al. 2022, Cosmological Information in the Marked Power Spectrum of the Galaxy Field, arXiv, doi: [10.48550/ARXIV.2206.01709](https://doi.org/10.48550/ARXIV.2206.01709)
- Matilla, J. M. Z., Sharma, M., Hsu, D., & Haiman, Z. 2020, *Physical Review D*, 102, doi: [10.1103/physrevd.102.123506](https://doi.org/10.1103/physrevd.102.123506)
- Murray, S. 2014, HMF: Halo Mass Function calculator, Astrophysics Source Code Library, record ascl:1412.006. <http://ascl.net/1412.006>
- Murray, S. G., Power, C., & Robotham, A. S. G. 2013, *Astronomy and Computing*, 3, 23, doi: [10.1016/j.ascom.2013.11.001](https://doi.org/10.1016/j.ascom.2013.11.001)
- Naidoo, K., Massara, E., & Lahav, O. 2022, Monthly Notices of the Royal Astronomical Society, 513, 3596, doi: [10.1093/mnras/stac1138](https://doi.org/10.1093/mnras/stac1138)
- Naidoo, K., Whiteway, L., Massara, E., et al. 2019, Monthly Notices of the Royal Astronomical Society, 491, 1709, doi: [10.1093/mnras/stz3075](https://doi.org/10.1093/mnras/stz3075)
- Pan, S., Liu, M., Forero-Romero, J., et al. 2020, Cosmological parameter estimation from large-scale structure deep learning. <https://arxiv.org/abs/1908.10590>
- Petri, A., Haiman, Z., Hui, L., May, M., & Kratochvil, J. M. 2013, *Phys. Rev. D*, 88, 123002, doi: [10.1103/PhysRevD.88.123002](https://doi.org/10.1103/PhysRevD.88.123002)
- Philcox, O. H., & Ivanov, M. M. 2022, *Physical Review D*, 105, doi: [10.1103/physrevd.105.043517](https://doi.org/10.1103/physrevd.105.043517)
- Porqueres, N., Heavens, A., Mortlock, D., & Lavaux, G. 2021, Monthly Notices of the Royal Astronomical Society, 509, 3194–3202, doi: [10.1093/mnras/stab3234](https://doi.org/10.1093/mnras/stab3234)
- Prelogović, D., Mesinger, A., Murray, S., Fiameni, G., & Gillet, N. 2021, Machine learning galaxy properties from 21 cm lightcones: impact of network architectures and signal contamination. <https://arxiv.org/abs/2107.00018>
- Press, W. H., & Schechter, P. 1974, *ApJ*, 187, 425, doi: [10.1086/152650](https://doi.org/10.1086/152650)
- Ramanah, D. K., Lavaux, G., Jasche, J., & Wandelt, B. D. 2019, *A&A*, 621, A69, doi: [10.1051/0004-6361/201834117](https://doi.org/10.1051/0004-6361/201834117)
- Rao, C. R. 1945, *Bulletin of the Calcutta Mathematical Society*, 37, 81–89
- Ravanbakhsh, S., Oliva, J., Fromenteau, S., et al. 2017, Estimating Cosmological Parameters from the Dark Matter Distribution. <https://arxiv.org/abs/1711.02033>
- Reed, D. S., Bower, R., Frenk, C. S., Jenkins, A., & Theuns, T. 2006, Monthly Notices of the Royal Astronomical Society, 374, 2, doi: [10.1111/j.1365-2966.2006.11204.x](https://doi.org/10.1111/j.1365-2966.2006.11204.x)
- Ribli, D., Armin Pataki, B., & Csabai, I. 2018, An improved cosmological parameter inference scheme motivated by deep learning. <https://arxiv.org/abs/1806.05995>
- Satorras, V. G., Hoogeboom, E., Fuchs, F. B., Posner, I., & Welling, M. 2021, E(n) Equivariant Normalizing Flows, arXiv, doi: [10.48550/ARXIV.2105.09016](https://doi.org/10.48550/ARXIV.2105.09016)
- Sutter, P. M., Lavaux, G., Wandelt, B. D., & Weinberg, D. H. 2012, *ApJ*, 761, 44, doi: [10.1088/0004-637X/761/1/44](https://doi.org/10.1088/0004-637X/761/1/44)
- Tegmark, M., Taylor, A. N., & Heavens, A. F. 1997, *The Astrophysical Journal*, 480, 22–35, doi: [10.1086/303939](https://doi.org/10.1086/303939)
- Ueda, H., & Itoh, M. 1997, *Publications of the Astronomical Society of Japan*, 49, 131, doi: [10.1093/pasj/49.2.131](https://doi.org/10.1093/pasj/49.2.131)
- Uhlemann, C., Friedrich, O., Villaescusa-Navarro, F., Banerjee, A., & Codis, S. 2020, *MNRAS*, 495, 4006, doi: [10.1093/mnras/staa1155](https://doi.org/10.1093/mnras/staa1155)

Uhlemann, C., Friedrich, O., Villaescusa-Navarro, F., Banerjee, A., & Codis, S. 2020, Monthly Notices of the Royal Astronomical Society, 495, 4006, doi: [10.1093/mnras/staa1155](https://doi.org/10.1093/mnras/staa1155)
van de Weygaert, R., Jones, B. J., & Martínez, V. J. 1992, Physics Letters A, 169, 145, doi: [https://doi.org/10.1016/0375-9601\(92\)90584-9](https://doi.org/10.1016/0375-9601(92)90584-9)
Villaescusa-Navarro, F., Wandelt, B. D., Anglés-Alcázar, D., et al. 2020a, Neural networks as optimal estimators to marginalize over baryonic effects. <https://arxiv.org/abs/2011.05992>
Villaescusa-Navarro, F., Hahn, C., Massara, E., et al. 2020b, The Astrophysical Journal Supplement Series, 250, 2, doi: [10.3847/1538-4365/ab9d82](https://doi.org/10.3847/1538-4365/ab9d82)

Villanueva-Domingo, P., & Villaescusa-Navarro, F. 2022, Learning cosmology and clustering with cosmic graphs, arXiv, doi: [10.48550/ARXIV.2204.13713](https://arxiv.org/abs/2204.13713)
Xu, X., Cisewski-Kehe, J., Green, S., & Nagai, D. 2019, Astronomy and Computing, 27, 34–52, doi: [10.1016/j.ascom.2019.02.003](https://doi.org/10.1016/j.ascom.2019.02.003)
Yang, D., & Yu, H.-B. 2022, A graph model for the clustering of dark matter halos, arXiv, doi: [10.48550/ARXIV.2206.05578](https://arxiv.org/abs/2206.05578)

APPENDIX

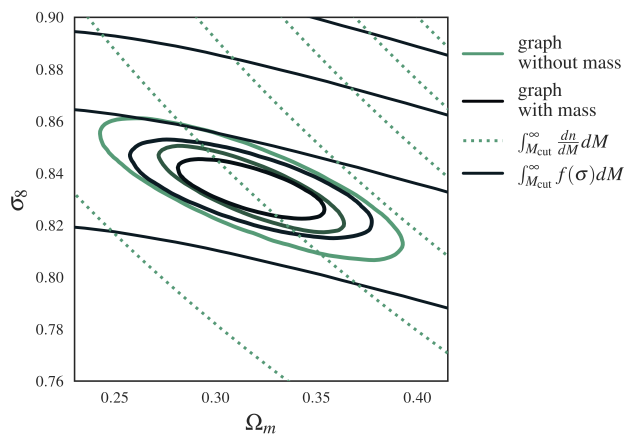


FIG. 9.— Comparison of undecorated graph (green ellipse) and decorated graph (dark ellipse) gIMNN Fishers, plotted over integrated halo number density (dashed green lines) and mass fraction (dark solid lines) functions from fixed M_{cut} . Decorating graphs with mass information induces a slight rotation away from dn/dM and towards $f(\sigma)$ contours, since this quantity incorporates both mass and halo number information.

COMPARING HALO MASS AND NUMBER DENSITY FUNCTIONS

Here we discuss the difference between the halo number density function and halo mass function in the context of gIMNN information extraction. The halo number density function,

$$\frac{dn}{dM} = \frac{\rho_o}{M} \frac{d \ln \sigma^{-1}(M)}{dM} f(\sigma), \quad (\text{A1})$$

and the halo mass function,

$$f(\sigma) = \frac{M}{\rho_o} \frac{dn(M)}{d \ln(\sigma^{-1}(M))}, \quad (\text{A2})$$

within the Press-Schechter formalism (Press & Schechter 1974). Integrating the halo number density from a fixed mass M_{cut} yields the number of halos with a mass above this threshold:

$$N(M_i > M_{\text{cut}}) = \int_{M_{\text{cut}}}^{\infty} \frac{dn}{dM} dM, \quad (\text{A3})$$

which in our case is the node cardinality of a halo graph, N^v . By contrast, integrating the halo mass function from M_{cut} yields the *fraction of total mass* residing in collapsed halos of mass above M_{cut} :

$$F(M_i > M_{\text{cut}}) = \int_{M_{\text{cut}}}^{\infty} f(\sigma) dM, \quad (\text{A4})$$

which incorporates *both* halo number N^v and mass information above M_{cut} .

We compare these two integrated quantities to undecorated and decorated gIMNN Fisher constraints in Figure 9. In the undecorated case (green ellipse), the network has explicit access to halo number and clustering information, resulting in contours more closely aligned with integrated dn/dM (dashed green lines). By contrast, when the graph nodes are annotated with mass labels (black ellipse), the network has explicit access to a combination of halo number, mass, and clustering information. This results in a slight rotation towards the integrated HMF $f(\sigma)$ contours (dark solid lines), since this quantity reflects the addition of mass fraction information. This effect is also illustrated in Figure 7. As discussed in Section 6, as noise level decreases, the network has access to sharper mass information, inducing a rotation towards the integrated HMF line.

DETAILS OF GRAPH ASSEMBLY IN JAX

Here we detail `Jax`-compatible graph assembly. `Jax` is a pseudo-compiled language, meaning arrays must have a pre-determined fixed length before sent to a GPU device for operations like gradient descent. We navigate this constraint by padding graph features by pre-determined fixed values, and masking features to assess information content in a modular fashion.

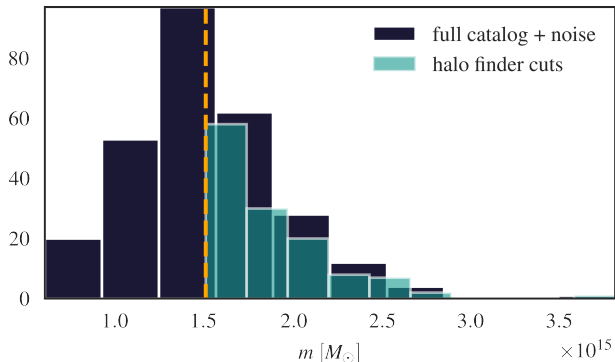


FIG. 10.— Mass distribution after added noise, $\sigma_{\text{noise}} = 0.2M_{\text{cut}}$ (black) and simulated halo finder cuts (teal) for a single fiducial simulation for masses larger than $1.1 \times 10^{15} M_\odot$. The orange dashed lines indicates the minimum mass considered by the “survey” cutoff, $M_{\text{cut}} = 1.5 \times 10^{15} M_\odot$.

The *Quijote* catalogues are assembled into graphs by first making a mass cut on a larger selection of halos. Masses are then padded with a pre-determined padding value, generally chosen to be $\max(N^v) + 10$. These dummy halos are assigned a very large mass value and a position outside of the 1Gpc^3 box. A distance matrix is then computed for *both* halo and dummy halo nodes, along with sender-receiver indexes, (s_k, r_k) . In the invariant graph case we also compute relative angles between all halos, outlined in Section 2.2.2. Connections $|\mathbf{d}_{ij}| > r_{\text{connect}}$ and $\mathbf{d}_{ij} = 0$ (self-edges) are then removed and replaced by a large padding value larger than r_{connect} . We compute N^e by the number of distances that fit these criteria. Distance values and sender-receiver arrays are then sorted smallest to largest and slotted into

padded arrays of length $\max(N^e) + 10$, where padded edge values are then replaced with zeros. We encountered gradient stability issues when padding was made too large for e.g. smaller edge sets, since more padding means the network is asked to operate on extra non-informative features. This sorting arrangement is advantageous since small distances (local connections) are always included in the halo graph’s edges, even if the padding container is chosen to be too small for all edges for a given r_{connect} value. What this means is that networks trained on a small r_{connect} can generalize reasonably well to datasets constructed with larger connection criteria.

Adding Noise. When constructing noisy catalogues on-the-fly, we first truncate catalogues with a smaller $M_{\text{cut}} = 1.1 \times 10^{15} M_\odot$ to include more halos in the true catalog. Every training epoch, a new realisation of observational noise is then added to the masses according to Section 6, after which halos below $M_{\text{cut}} = 1.5 \times 10^{15} M_\odot$ are discarded, illustrated in Figure 10. The graph edge attributes are then computed for the remaining halos as described above. For the noise scheme chosen in this work, this results in approximately equal numbers of halos being discarded above and below the mass cut line, yet increases the uncertainty in the informative HMF number count, which inflates constraints in Ω_m .

DETAILS OF THE GNN ARCHITECTURE

Masking Graph Features. To conduct information extraction tests with and without node decoration, the GNN architecture must remain fixed between decorated and undecorated cases. To mask a graph node or edge feature, an indicator $\mathbf{1}$ is assigned to the array in place of numerical value. These uninformative features are fed through the network but do not contribute to the information extraction since the same operation is performed across fiducial and derivative datasets, yet ensure a fair comparison of information as a function of catalogue data features since network architectures (hidden and output size dimensions) could be kept fixed with the same initialized weights.

This paper was built using the Open Journal of Astrophysics L^AT_EX template. The OJA is a journal which provides fast and easy peer review for new papers in the `astro-ph` section of the arXiv, making the reviewing process simpler for authors and referees alike. Learn more at <http://astro.theoj.org>.